Research Article Vol. 3, No. 4/25 August 2025/Optica Quantum 366

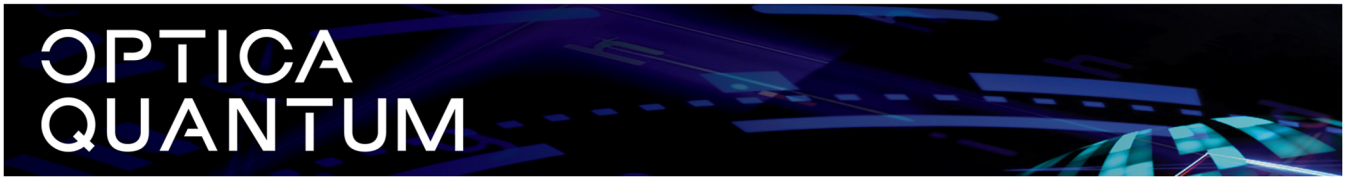

Continuous-variables cluster states in photonic time-crystals

M. Lyubarov,[1,2] A. Gorlach,[1,3] O. Segal,[1,3] M. Birk,[1,2] L. Nemirovsky-Levy,[1,2] Y. Plotnik,[1,2] and M. Segev[1,2,3,*]

[1]Solid State Institute, Technion, Haifa 32000, Israel
[2]Physics Department, Technion–Israel Institute of Technology, Haifa 32000, Israel
[3]Department of Electrical and Computer Engineering, Technion, Haifa 32000, Israel
*msegev@technion.ac.il

Received 27 January 2025; revised 23 May 2025; accepted 26 June 2025; published 29 July 2025

Photonic quantum computing has been rapidly advancing over the past decade, with measurement-based approaches emerging as particularly promising. A crucial requirement for these approaches is the generation of large-scale cluster states. In this work, we present a method to create cluster states using Photonic Time Crystals (PTCs)—dielectric materials with their refractive index rapidly modulated in time. PTCs effectively function as a set of optical parametric oscillators and beam-splitters, producing simultaneous two-mode squeezing for many pairs of photonic modes with opposite wavevectors. We utilize this capability to propose a method for generating two-dimensional cluster states, offering important advantages over existing protocols.

https://doi.org/10.1364/OPTICAQ.558274

1. INTRODUCTION

Quantum computing promises to perform computations based on principles of quantum mechanics and is lately getting increasing attention due to the potential to solve numerous practical problems that are intractable with classical computers [1,2]. Currently, there are many different physical platforms that are considered to be potential candidates for realizing quantum computing. Arguably, photonics is potentially the only platform that could be scaled to a million physical qubits. Yet photonics is also the most challenging of these platforms—because photons generally do not interact with one another, and realizing two-qubit gates at the single-photon level is highly problematic [3]. To overcome this problem, a different computational model, measurement-based quantum computing [4–6], has been suggested, circumventing the need for quantum gates. It uses only local measurements instead of unitary operations but requires a large-scale highly entangled initial state—a cluster state. The computation is then performed by successive adaptive measurements which teleport the initial logical state along the cluster and effectively apply to it the required unitary operations. Physically, each computational step in a cluster-state model is implemented by performing single-qubit measurements on selected photons in specific bases. The outcomes of these measurements determine the basis of the subsequent measurement (via feed-forward), effectively steering the computation [7].

Generation of a cluster state from single photons requires an optical scheme with a single-photon source and an entangling element. The element can be the source itself—in case of generation via semiconductor quantum dots [8–11] or via nonlinear optics [12,13]—or entanglement can be generated inside the photonic circuit after post-selection [14–17]. The scaling of these techniques is still an open technological challenge. The very weak strength of optical nonlinearities at the single-photon level, inevitable coupling losses and the need for post-selection, effectively make the generation of cluster states probabilistic, which is fundamentally unscalable. The alternative is to use the continuous variables (CV) approach—to encode quantum information in continuous photonic degrees of freedom, such as the electromagnetic field (EM) quadratures q, p [18–21], instead of using a discrete Hilbert space of qubits. This approach generates entanglement deterministically, making it attractive for scalable implementations. Cluster states based on CV [22–24] have now been widely implemented in experiments, with cluster states as large as tens of thousands of photonic modes being demonstrated [25–27].

The existing techniques for the generation of CV cluster states require optical schemes that consist of single-mode squeezers, beam-splitters, and/or quantum non-demolition coupling [14,15,23,28], with the modes comprising the cluster states being temporally separated. One of the key limitations in this technique of cluster state generation is the degree of squeezing achievable by optical parametric oscillators (OPOs) in experiments [21,23,29]. To achieve fault-tolerant quantum computing in the CV measurement-based scheme, one needs a source with at least 12.7 dB of squeezing [23,29,30], which is extremely hard to realize with current technologies.

Here, we propose a new way of generating cluster states by using Photonic Time Crystals (PTCs). PTCs are materials

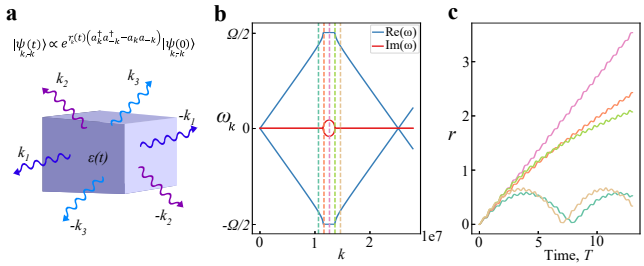

Fig. 1. The modes of a PTC. (a) Sketch of a 3D PTC medium, generating photon pairs in the modes with opposite momentum via two-mode squeezing. (b) Characteristic band structure of a PTC with bands and gaps in $\boldsymbol{k}$. The permittivity modulation is $\varepsilon(t) = \varepsilon_0 + \Delta\varepsilon \cdot sin(\Omega t)$, where $\varepsilon_0 = 1.5$, $\Delta\varepsilon = 0.5$, $T = 1fs$, $\Omega = 2\pi/T$. (c) Dynamics of the degree of squeezing in a PTC for the modes associated with the PTC band and with the PTC bandgap: the dynamics is oscillatory for the former (the wavenumber is associated with real values of the frequency) and monotonically increasing for the latter (the wavenumber is associated with complex values of the frequency).

with dielectric permittivity rapidly modulated in time [31,32]. The modulations of the permittivity, if sharp enough, result in time-reflected and time-refracted waves [33–38]. When the modulation is periodic on the time scale of an optical cycle, the time-reflected and time-refracted waves interfere and form a PTC, which displays a band structure in the momentum [32]. That is, the dispersion relation in a PTC comprises bands where the frequencies have real values, separated by momentum gaps for which the frequencies are complex. The existence of the momentum band structure in PTCs opens up a plethora of exciting physics. For example, PTCs enable time-domain topological edge states [39], they may be used to modify and control spontaneous emission [40,41], they give rise to Cherenkov radiation below the Cherenkov threshold [42], and can be used for making time-varying mirrors [43]. Furthermore, PTCs combined with spatial modulation of their permittivity form spatio-temporal photonic crystals [44,45], which exhibit mixed frequency-momentum band gaps [46,47], and can be the basis for non-reciprocal optical devices [48]. Spatio-temporal photonic crystals also support sub-, super-, and transluminal waves [49,50] and hold the promise for exploring four-dimensional optics [51]. Unlike conventional band structures in frequency (associated, e.g., with spatially periodic structures of atoms and with spatial photonic crystals), the modes associated with the momentum gaps of a PTC are exponentially amplified—drawing energy from the modulation, or attenuated—transferring energy to the modulation [40]. This is possible due to the absence of energy conservation in time-varying media. On the quantum level, the amplification of gap modes is manifested by two-mode squeezing (TMS): pairs of photons in modes with opposite wavevectors $\boldsymbol{k}$ and $-\boldsymbol{k}$ are generated during the modulation of the medium, as illustrated in Fig. 1(a). A pair of modes sharing TMS is a CV analogue of a Bell state, which can be used in quantum teleportation [52,53], dense coding [54], quantum key distribution [55], and more [56]. This TMS combined with the fact that it happens in all the modes residing in the momentum gap of the PTC is the key ingredient that makes PTCs, and in a broader sense, controlled time-varying dielectric media, a convenient candidate for numerous quantum information applications.

Here, we utilize the TMS property of PTCs to propose a mechanism for generation of optical CV cluster states. The creation of multi-mode TMS by PTCs, in fact, makes PTCs effectively equivalent to a set of multiple OPOs and beam-splitters. Employing PTCs to generate CV cluster states can overcome one of the main obstacles: the limited degree of squeezing generated by OPOs. In PTCs, the level of squeezing is defined only by the degree of control over the dielectric medium. In what follows, we briefly introduce the model we use for a PTC through classical electrodynamics by deriving PTC band structure and eigenmodes. We then turn to the quantum picture, discuss the PTC Hamiltonian, and explain the effect of the PTC on the bosonic modes in the quantum regime. Finally, we present the proposal to generate a CV cluster state by exploiting the quantum properties of PTCs and compare it to other techniques of generating CV cluster states.

2. CLASSICAL AND QUANTUM MODELS OF EMISSION FROM A PTC

We use a model of a homogeneous time-varying medium with periodic dielectric permittivity $\varepsilon(t) = \varepsilon(t+T)$. We can describe it with Maxwell equations:

$$\nabla \times H = \frac{1}{c}\frac{\partial(\varepsilon(t)E)}{\partial t}, \tag{1.1}$$

$$\nabla \times E = -\frac{1}{c}\frac{\partial H}{\partial t}. \tag{1.2}$$

From Eqs. (1.1) and (1.2) and using spatial Fourier transform $H_k \propto \int H e^{i\boldsymbol{k}\boldsymbol{r}} d^3\boldsymbol{r}$, we can construct the wave equation for H_k

$$-\partial_t(\varepsilon(t)\partial_t H_k) = c^2k^2H_k. \tag{1.3}$$

Equation (1.3) has Floquet eigenmodes, i.e., periodic solutions of the form $H_k(t) = A_k(t)\, e^{-i\omega_k t}$, where $A_k(t) = A_k(t+T)$, and ω_k is called a Floquet eigenfrequency. The typical dispersion curve in a PTC, i.e., the function $\omega_k(k)$, is shown in Fig. 1(b). In the k-bands, ω_k is real, and the eigenmodes are reminiscent of monochromatic plane waves, but in the k-gaps, the ω_k is complex, and the eigenmodes are exponentially growing and decaying waves. Thus, in the k-gaps, the number of photons in each mode grows exponentially with time. The degree of squeezing in a mode is closely related to the number of photons ($\langle n\rangle \sim sinh^2 r$ for squeezed vacuum, where $\langle n\rangle$ is the mean number of photons, r is the degree of squeezing. Squeezing in the modes of a PTC follows the same trend: for modes in the band, the degree of squeezing oscillates near zero, while for gap modes, it grows monotonically, as shown in Fig. 1(c). The degree of two-mode squeezing r can be converted to decibel scale as $S\,[\mathrm{dB}] = 10\log_{10}\left(e^{2r}\right) \approx 8.7 \cdot r$. Thus, to achieve the threshold of 12.7 dB with PTC, one should reach the value of squeezing degree $r \approx 1.46$. For the specific case of the PTC shown in Figs. 1(b) and 1(c), this value for the mode in the center of the gap is achieved after the duration of $5\,T$. Importantly, the exponentially growing modes in a PTC are actually physical, as they draw their energy from the modulation constructing the PTC. That is, the modulation of ε in time requires pumping the system with energy, and the waves with k in the gap draw energy from this modulation in each cycle.

To explain the action of a PTC on the EM waves from the quantum perspective, we can analyze the PTC Hamiltonian (see [40–42])

$$\hat{H} = \sum_{\boldsymbol{k}} \hbar(\omega_k(t)(\hat{a}^\dagger_{\boldsymbol{k}}\hat{a}_{\boldsymbol{k}} + \hat{a}^\dagger_{-\boldsymbol{k}}\hat{a}_{-\boldsymbol{k}}) + g_k(t)(\hat{a}^\dagger_{\boldsymbol{k}}\hat{a}^\dagger_{-\boldsymbol{k}} + \hat{a}_{-k}\hat{a}_k)), \quad \textbf{(1.4)}$$

$$\omega_k(t) = \frac{ck}{n(t)}\frac{\frac{n(t)}{n_r} + \frac{n_r}{n(t)}}{2}, \quad \textbf{(1.5)}$$

$$g_k(t) = \frac{ck}{n(t)}\frac{\frac{n(t)}{n_r} - \frac{n_r}{n(t)}}{2}. \quad \textbf{(1.6)}$$

Here, $\hat{a}^\dagger_k(\hat{a}_k)$ are the creation (annihilation) operators in mode $\boldsymbol{k}$, and n_r is the average refractive index throughout the modulation cycle. The first term in Eq. (1.4) is the ordinary photon number term with a time-varying frequency, while the second term is responsible for the two-mode squeezing (TMS) for pairs of modes with opposite $\boldsymbol{k}$. Due to the structure of the Hamiltonian, only modes with opposite wavevectors $\boldsymbol{k}, -\boldsymbol{k}$ are coupled with each other, while every pair of waves is propagating independently from all other modes. The Hamiltonian (1.4) conserves momentum, but does not conserve the number of photons, and its eigenmodes display a band-structure behavior which is the same as a classical EM field in the eigenmode equation (1.3). Namely, for k-vector in the band of a PTC, one can construct the Floquet eigenmodes $|\psi_k\rangle = |\phi_k\rangle e^{-i\omega_k t}$. For k-vector in the gap of the PTC, no eigenmodes exist, but the number of photons grows exponentially with time, following the classical intuition. The degree of TMS produced by Hamiltonian (1.4) also depends on whether we consider a band mode or a gap mode (see Fig. 1(c)). For band modes, the TMS oscillates near zero, but for gap modes, the squeezing grows linearly with time and is limited only by the duration of the PTC, i.e., how accurately and for how long we are able to modulate the permittivity.

3. BLOCH–MESSIAH DECOMPOSITION OF A PTC

We can analyze the action of the Hamiltonian (1.4) on the EM field modes in the optical phase space. By introducing the field quadrature operators q, p for the mode with wavevector $\boldsymbol{k}$ as

$$\hat{q}_{\boldsymbol{k}} = \frac{\hat{a}_{\boldsymbol{k}} + \hat{a}^\dagger_{\boldsymbol{k}}}{\sqrt{2}}, \quad \hat{p}_{\boldsymbol{k}} = i\frac{\hat{a}^\dagger_{\boldsymbol{k}} - \hat{a}_{\boldsymbol{k}}}{\sqrt{2}}. \quad \textbf{(1.7)}$$

We can rewrite the Hamiltonian (1.4) in matrix form as

$$\hat{H} = \sum_{\boldsymbol{k}} \tfrac{1}{2}\hat{\mathbf{r}}_{\boldsymbol{k}} H_k \hat{\mathbf{r}}_{\boldsymbol{k}}; \quad \hat{\mathbf{r}}_{\boldsymbol{k}} = \begin{pmatrix} \hat{q}_{\boldsymbol{k}} \\ \hat{p}_{\boldsymbol{k}} \\ \hat{q}_{-\boldsymbol{k}} \\ \hat{p}_{-\boldsymbol{k}} \end{pmatrix}$$
$$H_k(t) = \omega_k(t) I + g_k(t) \begin{pmatrix} 0 & 0 & 1 & 0 \\ 0 & 0 & 0 & -1 \\ 1 & 0 & 0 & 0 \\ 0 & -1 & 0 & 0 \end{pmatrix} \quad \textbf{(1.8)}$$

where I is a 4×4 unit matrix. The Hamiltonian (1.8) is Gaussian, i.e., it is second order in q, p, and the quantum states of the system can be described by the mean values of quadratures $\langle\hat{\mathbf{r}}_{\boldsymbol{k}}\rangle$ and their correlations. The evolution of the quantum state of two modes $\boldsymbol{k}$ and $-\boldsymbol{k}$ can then be described through

$$\frac{\partial\hat{\mathbf{r}}_{\boldsymbol{k}}}{\partial t} = \Omega H_k(t)\hat{\mathbf{r}}_{\boldsymbol{k}}; \quad \frac{\partial V_k}{\partial t} = \Omega H_k(t) V_k - V_k H_k(t)\Omega, \quad \textbf{(1.9)}$$

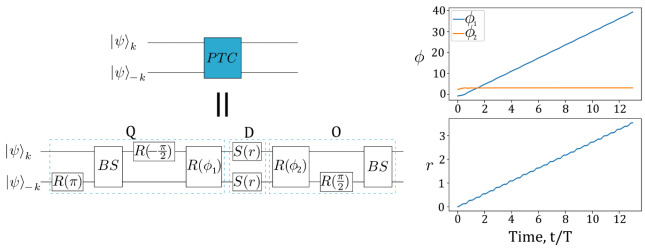

Fig. 2. The Bloch–Messiah decomposition of a PTC. Left: Bloch–Messiah decomposition of the PTC modulation applied to a pair of modes with opposite wavevectors $\{\boldsymbol{k}, -\boldsymbol{k}\}$ into the elements of the optical scheme. Right: Dynamics of the three parameters of the decomposition for $k \in$ PTC gap: two single-mode rotation phases (top) and the degree of squeezing (bottom).

where $(V_k)_{ij} = \langle(\hat{\mathbf{r}}_{\boldsymbol{k}})_i(\hat{\mathbf{r}}_{\boldsymbol{k}})_j\rangle - \langle(\hat{\mathbf{r}}_{\boldsymbol{k}})_i\rangle\langle(\hat{\mathbf{r}}_{\boldsymbol{k}})_j\rangle$ is a covariance matrix, and Ω is a commutation matrix, $[(\hat{\mathbf{r}}_{\boldsymbol{k}})_i, (\hat{\mathbf{r}}_{\boldsymbol{k}})_j] = i\Omega_{ij}$. Since the Hamiltonian is time-dependent, the solution of (1.9) cannot be found straightforwardly, but we can generally express it as

$$\hat{\mathbf{r}}_{\boldsymbol{k}}(t) = U(t)\hat{\mathbf{r}}_{\boldsymbol{k}}(0), \quad \textbf{(1.10)}$$

where $U(t)$ is a Gaussian unitary transformation on the quantum state of two modes $\boldsymbol{k}$ and $-\boldsymbol{k}$ due to the modulation of the medium by the PTC. We can calculate this $U(t)$ numerically and apply to it a Bloch–Messiah decomposition [57]

$$U(t) = O(t)D(t)Q(t), \quad \textbf{(1.11)}$$

where $O(t), Q(t)$ are passive two-mode transformations and $D(t)$ is the squeezing operation. The Bloch–Messiah decomposition allows to decompose the action of the PTC on the optical modes into the sequence of operations—such as single-mode squeezing, mode mixing, and phase shifts—that can be implemented by basic optical elements. $D(t)$ represents single-mode squeezing, which is usually generated by an OPA, and the passive transformations $O(t), Q(t)$ can be realized by delay lines and beam-splitters. This decomposition for the PTC is illustrated on the left side of Fig. 2. It contains several local and global phase shifts, two in-line squeezers, and two beam-splitters—one before and one after the squeezing. The decomposition has three parameters that vary over time—two phases ϕ_1, ϕ_2, and, more importantly, the squeezing degree r. Their dynamics for two modes $\boldsymbol{k}, -\boldsymbol{k}$ associated with the k-gap are shown on the right side of Fig. 2. One can see that the squeezing degree grows linearly for the gap mode (the squeezing in Fig. 2 is the same as in Fig. 1(c) for the mode in the center of the gap). The circuit in Fig. 2 generates TMS, and the longer the PTC acts on the system—the higher the squeezing degree is for the modes. For $|\psi(t=0)\rangle_{\boldsymbol{k},-\boldsymbol{k}} = |vac\rangle_{\boldsymbol{k}} \otimes |vac\rangle_{-\boldsymbol{k}}$, the state of each pair of modes acted on by the PTC is of two-mode squeezed vacuum, which turns into a Bell state in the $t \to \infty$ limit.

4. GENERATION OF CLUSTER STATES USING A PTC

The effect of the PTC applied to a vacuum state is very similar to the initial part of the cluster state generation process via a dual-rail mechanism [25–27]. Namely, each TMS pair $\{\boldsymbol{k_i}, -\boldsymbol{k_i}\}$ generated by the PTC is equivalent to the generation of one pair of single-mode squeezed vacuum pulses entangled on a beam-splitter. This equivalence allows the implementation of the

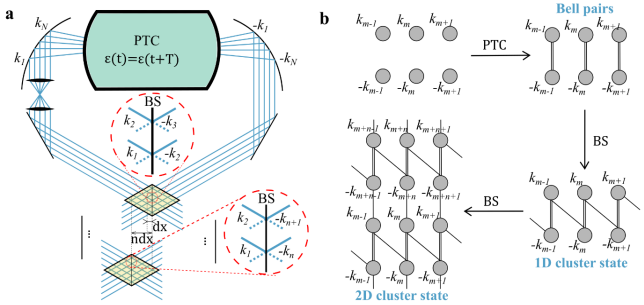

Fig. 3. Generation of a 2D cluster state using a PTC. (a) Conceptual illustration of the experimental setup. A PTC medium acts as a source generating a set of pairs of TMS modes with opposite wavevectors, which are then balanced on the first and the second beam-splitters in different pairs to generate 1D and 2D cluster states, respectively. (b) Structure of the generated cluster state.

whole generation mechanism in a simple optical scheme containing a PTC (Fig. 3(a)). A sample with a PTC medium inside generates multiple TMS pairs of modes with opposite wavevectors $\{\mathbf{k}_i, -\mathbf{k}_i\}_{i=1}^{N}$. After the PTC modulation stops, the modes with positive, $\{\mathbf{k}_i\}_{i=1}^{N}$, and negative, $\{-\mathbf{k}_i\}_{i=1}^{N}$, wavevectors start propagating towards the left side and the right side, respectively. Two curved mirrors after the PTC medium make the sets of waves incident from the right (left) parallel to each other. Then, we balance all the modes on a wide beam-splitter, creating an entangled chain (1D cluster state). The beam-splitter should be positioned to mix the modes with positive and negative wavevectors with a one-mode shift compared to their initial coupling inside the PTC (Fig. 3(a)). Finally, we balance the right and the left set of modes on another beam-splitter, with a longer n-mode shift. The n-mode shift can again be realized by carefully choosing the position of the beam-splitter (Fig. 3(a)). For every pair of modes, the PTC implements the circuit from Fig. 2. Note that we can omit the global phase shifts and the first passive two-mode unitary $Q(t)$, since it does not affect the initial vacuum state. The multi-mode state after the final beam-splitter is equivalent to a two-dimensional CV cluster state (Fig. 3(b)). To verify this, we calculate the nullifiers—linear combinations of quadrature operators that give zero when applied to a cluster state—for the multi-mode quantum state after propagating through the setup. For the Gaussian state implemented by the circuit in Fig. 3(c), in the limit of infinite squeezing, the nullifiers are

$$\begin{aligned} N_{i,x} &= x_{-k_{m-1}} + x_{k_{m-n-1}} + x_{k_m} - x_{-k_{m+n}} + x_{-k_m} + x_{k_{m-n}} \\ &\quad - x_{-k_{m+1}} + x_{-k_{m+n+1}} \\ N_{i,p} &= p_{-k_{m-1}} + p_{k_{m-n-1}} + p_{k_m} - p_{-k_{m+n}} - p_{-k_m} - p_{k_{m-n}} \\ &\quad + p_{-k_{m+1}} - p_{-k_{m+n+1}} \end{aligned} \tag{1.12}$$

The nullifiers (1.12) satisfy the standard nullifier property $\left[N_{i,x(p)}, N_{j,x(p)}\right] = 0$. The nullifiers for the pair of modes $\boldsymbol{k}_i, \boldsymbol{k}_{-i}$ contain only quadratures of the modes from the adjacent pairs, mixed with modes $\boldsymbol{k}_i, \boldsymbol{k}_{-i}$ by the beam-splitters, indicating a cluster-like nearest neighbor coupling.

5. COMPARISON TO EXISTING METHODS OF OPTICAL CLUSTER STATE GENERATION

After explaining our PTC-based mechanism, it is important to compare its expected performance to the commonly used SPDC-based technique. Thus far, PTCs have been demonstrated only at RF frequencies [32] and very recently with microwaves [58], while PTCs at optical frequencies are yet to be realized. For this reason, we can compare only to idealized cases. We therefore compare an ideal PTC with an ideal SPDC process, for the purpose of generating cluster states.

From the outset, we note that generating two-mode squeezing (TMS) with a PTC has a fundamental advantage over squeezing via SPDC: dimensionality. As described above, in a PTC, pairs of entangled photons are generated at high rates, for all modes residing in the momentum gap with no need for phase-matching and in all directions. On the other hand, the SPDC process is restricted by phase-matching and by the propagation direction of the pump. Essentially, in the context of generating pairs of entangled photons, one may think of a PTC as a dispersionless OPA (which inside a cavity becomes an OPO) pumped from all directions. Thus, the dimensionality of the set of modes amplified by the SPDC process is 1, and even that is restricted by phase-matching, whereas the dimensionality of the amplified gap modes in a PTC is 3, with no further restriction imposed by phase-matching.

Other advantages of the PTC-based setting for generating cluster states relate to the system architecture, as illustrated in Fig. 3, compared to the conventional SPDC-based dual-rail implementations. The latter typically uses temporal mode separation, which makes them vulnerable to temporal decoherence and information loss across the qubit chain. In contrast, our approach employs spatial multiplexing of modes, thus eliminating temporal decoherence. More importantly, with temporal mode separation, the number of input modes is set by the delay line ratio—the ratio between the repetition rate of the pulsed source and the length of the overarching delay line. Increasing the number of input modes in such a system requires one to develop squeezed pulse sources with higher bandwidth and repetition rates, or more trivially to increase the length of the delay line. However, increasing the delay line length increases losses which degrade entanglement, placing an inherent limit on the number of input modes. In contrast, the PTC scheme proposed here does not have this inherent limit—the choice of number of input modes directly dictates the location of the second beam-splitter, but there is no loss or phase decoherence that scales with this number. Another advantage of PTCs is that, unlike SPDC systems—where increasing the nonlinear crystal length boosts gain but simultaneously degrades phase-matching across multiple modes due to phase-mismatch scaling with the cavity length—PTCs are not subject to this trade-off, as they do not rely on phase-matching mechanisms.

The analogy of the setting described here to cluster state generation via frequency comb mechanisms is worth mentioning. Our setup spatially separates modes associated with k-vectors, while the optical frequency comb techniques [59–62] generate cluster states with temporally separated modes associated with different frequencies. In principle, the analogous idea of generating momentum combs via diffraction grating can be combined with our PTC proposal to yield cluster states of an even higher dimension.

6. CONCLUSION

In this work, we have presented the idea of utilizing a PTC for generating continuous-variable cluster states of photons. The

utility comes from the fact that temporal variations of a homogeneous medium act as two-mode squeezing, for many pairs of EM modes simultaneously. We used this property to propose a mechanism for the generation of cluster states from a PTC in a simple optical setup. Importantly, the proposed cluster state is two-dimensional due to the passes through two entangling beam-splitters, but the dimensionality of the cluster can also be increased by increasing the dimensionality of the set of k-vectors. For example, if a PTC source generates modes with k-vectors within a finite spherical angle, then the set of the modes alone will be two-dimensional, and consequently, the generated cluster state can be three-dimensional in the same setup with two beam-splitters.

We have outlined several potential advantages of photonic time crystals (PTCs) over conventional SPDC-based methods for cluster state generation and proposed a corresponding generation scheme. While a direct comparison with existing OPO-based implementations is not yet feasible—since PTCs have been thus far experimentally realized only at RF frequencies and microwaves—the theoretical advantages (comparing idealized schemes) are compelling. Realizing PTCs in the lab requires the ability to manipulate a dielectric medium on the timescale of a single cycle, which, at optical frequencies, means strong modulation of the refractive index within just a few femtoseconds. Although this was long considered impractical, recent advancements have demonstrated promising methods for achieving ultrafast permittivity modulation through epsilon-near-zero (ENZ) materials, specifically using transparent conductive oxides (TCOs) [63–67]. Notably, time refraction has already been observed within femtosecond scales in indium tin oxide (ITO) [68,69], and time reflection is expected to be demonstrated soon. This progress suggests that testing the concepts discussed here could become feasible in the coming years. In fact, at microwave frequencies, these ideas are already within reach, following the recent observations of time reflection at sub-GHz frequencies [38,70] and the recent experiments observing a PTC [58]. Another alternative, also in microwaves, relies on vibration–rotation transitions in molecules [71].

Funding. Israel Science Foundation; Air Force Office of Scientific Research (2032635: FA8655-22-1-7256).

Disclosures. The authors declare no conflicts of interest.

Data availability. No data were generated or analyzed in the presented research.

REFERENCES

1. P. W. Shor, "Algorithms for quantum computation: discrete logarithms and factoring," in Proceedings of the 35th Annual Symposium on Foundations of Computer Science (FOCS) (1994), pp. 124–134.
2. L. K. Grover, "A fast quantum mechanical algorithm for database search," presented at the *28th Annual ACM Symposium on Theory of Computing*, Association for Computing Machinery, New York, NY, USA, 1996, pp. 212–219.
3. G. Moody, V. J. Sorger, D. J. Blumenthal, *et al.*, "2022 Roadmap on integrated quantum photonics," J. Phys. Photon. **4**(1), 012501 (2022).
4. R. Raussendorf and H. J. Briegel, "A one-way quantum computer," Phys. Rev. Lett. **86**(22), 5188–5191 (2001).
5. H. J. Briegel and R. Raussendorf, "Persistent entanglement in arrays of interacting particles," Phys. Rev. Lett. **86**(5), 910–913 (2001).
6. P. Walther, K. J. Resch, T. Rudolph, *et al.*, "Experimental one-way quantum computing," Nature **434**(7030), 169–176 (2005).
7. K. Alexander, A. Bahgat, A. Benyamini, *et al.*, "A manufacturable platform for photonic quantum computing," arXiv (2024).
8. N. H. Lindner and T. Rudolph, "Proposal for pulsed on-demand sources of photonic cluster state strings," Phys. Rev. Lett. **103**(11), 113602 (2009).
9. I. Schwartz, D. Cogan, E. R. Schmidgall, *et al.*, "Deterministic generation of a cluster state of entangled photons," Science **354**(6311), 434–437 (2016).
10. D. Cogan, Z.-E. Su, O. Kenneth, *et al.*, "Deterministic generation of indistinguishable photons in a cluster state," Nat Photon. **17**(4), 324–329 (2023).
11. V. S. Ferreira, G. Kim, A. Butler, *et al.*, "Deterministic generation of multidimensional photonic cluster states with a single quantum emitter," Nat. Phys. **20**(5), 865–870 (2024).
12. C.-Y. Lu, X.-Q. Zhou, O. Gühne, *et al.*, "Experimental entanglement of six photons in graph states," Nat. Phys. **3**(2), 91–95 (2007).
13. B. A. Bell, D. A. Herrera-Martí, M. S. Tame, *et al.*, "Experimental demonstration of a graph state quantum error-correction code," Nat. Commun. **5**(1), 3658 (2014).
14. Y. Pilnyak, N. Aharon, D. Istrati, *et al.*, "Simple source for large linear cluster photonic states," Phys. Rev. A **95**(2), 022304 (2017).
15. D. Istrati, Y. Pilnyak, J. C. Loredo, *et al.*, "Sequential generation of linear cluster states from a single photon emitter," Nat. Commun. **11**(1), 5501 (2020).
16. P. Thomas, L. Ruscio, O. Morin, *et al.*, "Fusion of deterministically generated photonic graph states," Nature **629**(8012), 567–572 (2024).
17. P. G. Kwiat, K. Mattle, H. Weinfurter, *et al.*, "New high-intensity source of polarization-entangled photon pairs," Phys. Rev. Lett. **75**(24), 4337–4341 (1995).
18. D. Gottesman, A. Kitaev, and J. Preskill, "Encoding a qubit in an oscillator," Phys. Rev. A **64**(1), 012310 (2001).
19. S. Lloyd and S. L. Braunstein, "Quantum computation over continuous variables," Phys. Rev. Lett. **82**(8), 1784–1787 (1999).
20. C. Weedbrook, S. Pirandola, R. García-Patrón, *et al.*, "Gaussian quantum information," Rev. Mod. Phys. **84**(2), 621–669 (2012).
21. K. Fukui and S. Takeda, "Building a large-scale quantum computer with continuous-variable optical technologies," J. Phys. B: At. Mol. Opt. Phys. **55**(1), 012001 (2022).
22. N. C. Menicucci, "Temporal-mode continuous-variable cluster states using linear optics," Phys. Rev. A **83**(6), 062314 (2011).
23. N. C. Menicucci, "Fault-tolerant measurement-based quantum computing with continuous-variable cluster states," Phys. Rev. Lett. **112**(12), 120504 (2014).
24. C. Roh, G. Gwak, Y.-D. Yoon, *et al.*, "Generation of three-dimensional cluster entangled state," Nat. Photon. **19**(5), 526–532 (2025).
25. S. Yokoyama, R. Ukai, S. C. Armstrong, *et al.*, "Ultra-large-scale continuous-variable cluster states multiplexed in the time domain," Nat. Photon. **7**(12), 982–986 (2013).
26. M. V. Larsen, X. Guo, C. R. Breum, *et al.*, "Deterministic generation of a two-dimensional cluster state," Science **366**(6463), 369–372 (2019).
27. W. Asavanant, Y. Shiozawa, S. Yokoyama, *et al.*, "Generation of time-domain-multiplexed two-dimensional cluster state," Science **366**(6463), 373–376 (2019).
28. P. Van Loock, C. Weedbrook, and M. Gu, "Building Gaussian cluster states by linear optics," Phys. Rev. A **76**(3), 032321 (2007).
29. B. W. Walshe, L. J. Mensen, B. Q. Baragiola, *et al.*, "Robust fault tolerance for continuous-variable cluster states with excess antisqueezing," Phys. Rev. A **100**(1), 010301 (2019).
30. M. V. Larsen, C. Chamberland, K. Noh, *et al.*, "Fault-tolerant continuous-variable measurement-based quantum computation architecture," PRX Quant. **2**(3), 030325 (2021).
31. J. R. Zurita-Sánchez, P. Halevi, and J. C. Cervantes-González, "Reflection and transmission of a wave incident on a slab with a time-periodic dielectric function $\epsilon(t)$," Phys. Rev. A **79**(5), 053821 (2009).
32. J. R. Reyes-Ayona and P. Halevi, "Observation of genuine wave vector (k or β) gap in a dynamic transmission line and temporal photonic crystals," Appl. Phys. Lett. **107**(7), 074101 (2015).

33. F. R. Morgenthaler, "Velocity modulation of electromagnetic waves," IEEE Trans. Microw. Theory Tech. **6**(2), 167–172 (1958).
34. R. Fante, "Transmission of electromagnetic waves into time-varying media," IEEE Trans. Antennas Propag. **19**(3), 417–424 (1971).
35. J. T. Mendonça and P. K. Shukla, "Time refraction and time reflection: Two basic concepts," Phys. Scr. **65**(2), 160–163 (2002).
36. A. Shaltout, A. Kildishev, and V. Shalaev, "Time-varying metasurfaces and Lorentz non-reciprocity," Opt. Mater. Express **5**(11), 2459–2467 (2015).
37. T. R. Jones, A. V. Kildishev, M. Segev, *et al.*, "Time-reflection of microwaves by a fast optically-controlled time-boundary," Nat. Commun. **15**(1), 6786 (2024).
38. H. Moussa, G. Xu, S. Yin, *et al.*, "Observation of temporal reflection and broadband frequency translation at photonic time interfaces," Nat. Phys. **19**(6), 863–868 (2023).
39. E. Lustig, Y. Sharabi, and M. Segev, "Topological aspects of photonic time crystals," Optica **5**(11), 1390–1395 (2018).
40. M. Lyubarov, Y. Lumer, A. Dikopoltsev, *et al.*, "Amplified emission and lasing in photonic time crystals," Science **377**(6604), 425–428 (2022).
41. M. Lyubarov, A. Dikopoltsev, O. Segal, *et al.*, "Controlling spontaneous emission through the preparation of a photonic time-crystal," Opt. Express **32**(22), 39734–39742 (2024).
42. A. Dikopoltsev, Y. Sharabi, M. Lyubarov, *et al.*, "Light emission by free electrons in photonic time-crystals," Proc. Natl. Acad. Sci. USA **119**(6), e2119705119 (2022).
43. R. Tirole, E. Galiffi, J. Dranczewski, *et al.*, "Saturable time-varying mirror based on an epsilon-near-zero material," Phys. Rev. Appl. **18**(5), 054067 (2022).
44. F. Biancalana, A. Amann, A. V. Uskov, *et al.*, "Dynamics of light propagation in spatiotemporal dielectric structures," Phys. Rev. E Stat. Nonlin. Soft Matter. Phys. **75**(4 Pt 2), 046607 (2007).
45. C. Caloz and Z.-L. Deck-Leger, "Spacetime metamaterials—part I: General concepts," IEEE Trans. Antennas Propag. **68**(3), 1569–1582 (2020).
46. Y. Sharabi, A. Dikopoltsev, E. Lustig, *et al.*, "Spatiotemporal photonic crystals," Optica **9**(6), 585–592 (2022).
47. J. Park and B. Min, "Spatiotemporal plane wave expansion method for arbitrary space–time periodic photonic media," Opt. Lett. **46**(3), 484–487 (2021).
48. D. L. Sounas and A. Alù, "Non-reciprocal photonics based on time modulation," Nat. Photon. **11**(12), 774–783 (2017).
49. E. Galiffi, P. A. Huidobro, and J. B. Pendry, "Broadband nonreciprocal amplification in luminal metamaterials," Phys. Rev. Lett. **123**(20), 206101 (2019).
50. P. A. Huidobro, E. Galiffi, S. Guenneau, *et al.*, "Fresnel drag in space–time-modulated metamaterials," Proc. Natl. Acad. Sci. USA **116**(50), 24943–24948 (2019).
51. N. Engheta, "Four-dimensional optics using time-varying metamaterials," Science **379**(6638), 1190–1191 (2023).
52. L. Vaidman, "Teleportation of quantum states," Phys. Rev. A **49**(2), 1473–1476 (1994).
53. S. L. Braunstein and H. J. Kimble, "Teleportation of continuous quantum variables," Phys. Rev. Lett. **80**(4), 869–872 (1998).
54. S. L. Braunstein and H. J. Kimble, "Dense coding for continuous variables," Phys. Rev. A **61**(4), 042302 (2000).
55. S. Pirandola, S. Mancini, S. Lloyd, *et al.*, "Continuous-variable quantum cryptography using two-way quantum communication," Nat. Phys. **4**(9), 726–730 (2008).
56. S. L. Braunstein and P. van Loock, "Quantum information with continuous variables," Rev. Mod. Phys. **77**(2), 513–577 (2005).
57. S. L. Braunstein, "Squeezing as an irreducible resource," Phys. Rev. A **71**(5), 055801 (2005).
58. T. R. Jones, L. Prokopeva, A. V. Kildishev, *et al.*, "Observation of photonic time-crystal at microwave frequencies," in preparation (2025).
59. P. Du, Y. Wang, K. Liu, *et al.*, "Generation of large-scale continuous-variable cluster states multiplexed both in time and frequency domains," Opt. Express **31**(5), 7535–7544 (2023).
60. R. N. Alexander, P. Wang, N. Sridhar, *et al.*, "One-way quantum computing with arbitrarily large time-frequency continuous-variable cluster states from a single optical parametric oscillator," Phys. Rev. A **94**(3), 032327 (2016).
61. M. Chen, N. C. Menicucci, and O. Pfister, "Experimental realization of multipartite entanglement of 60 modes of a quantum optical frequency comb," Phys. Rev. Lett. **112**(12), 120505 (2014).
62. X. Liu, R. Yang, J. Zhang, *et al.*, "Generation of multipartite entangled states based on a double-longitudinal-mode cavity optomechanical system," Opt. Express **31**(19), 30005–30019 (2023).
63. M. Z. Alam, I. De Leon, and R. W. Boyd, "Large optical nonlinearity of indium tin oxide in its epsilon-near-zero region," Science **352**(6287), 795–797 (2016).
64. L. Caspani, R. P. M. Kaipurath, M. Clerici, *et al.*, "Enhanced nonlinear refractive index in ε-near-zero materials," Phys. Rev. Lett. **116**(23), 233901 (2016).
65. N. Kinsey, C. DeVault, A. Boltasseva, *et al.*, "Near-zero-index materials for photonics," Nat. Rev. Mater. **4**(12), 742–760 (2019).
66. W. Jaffray, F. Belli, Enrico G. Carnemolla, *et al.*, "Near-zero-index ultra-fast pulse characterization," Nat. Commun. **13**(1), 3536 (2022)
67. M. Clerici, N. Kinsey, C. DeVault, *et al.*, "Controlling hybrid nonlinearities in transparent conducting oxides via two-colour excitation," Nat. Commun. **8**, 15829 (2017).
68. E. Lustig, O. Segal, S. Saha, *et al.*, "Time-refraction optics with single cycle modulation," Nanophotonics **12**(12), 2221–2230 (2023).
69. R. Tirole, S. Vezzoli, E. Galiffi, *et al.*, "Double-slit time diffraction at optical frequencies," Nat. Phys. **19**(7), 999–1002 (2023).
70. T. R. Jones, A. V. Kildishev, M. Segev, *et al.*, "Time-reflection of microwaves by a fast optically-controlled time-boundary," arXiv (2023).
71. B. H. Bransden and C. J. Joachain, *Physics of Atoms and Molecules* (Pearson Education India, 2003).